J. Biomed. Eng. Res : 364-370, 2008

Digital Tomosynthesis using a Flat-panel Detector based Micro-CT

Koushik Kanti Mandal, Jeong Min Choi, Min Hyoung Cho, Soo Yeol Lee

Dept. of Biomedical Engineering, Kyung Hee University, Korea
(Received July 21, 2008. Accepted September 17, 2008)

Abstract

Recent development in large area flat-panel x-ray detector technology enables clinical application of digital tomosyntesis. Unlike conventional motion tomography using x-ray films, flat-panel x-ray detectors provide projection images in digital formats so that tomographic images can be synthesized in a more flexible way. For the digital tomosynthesis, precise movements of the x-ray source and the x-ray detector with respect to a fulcrum point are necessary. In this study, we apply the digital tomosynthesis technique to the flat-panel detector based micro-CT in which the flat-panel detector and the x-ray source rotate together on a circular arc. The experimental results suggest that flat-panel detector based 3D CTs can be used for digital tomosynthesis in the clinical environment.

Key words : digital tomosynthesis, micro-CT, cone-beam CT, flat-panel detector, shift-and-add algorithm

Ⅰ. INTRODUCTION

Digital tomosynthesis is a procedure that enables tomographic imaging by acquiring a limited number of projection images from a narrow angular range, and combining these projection images to reconstruct a quasi-three dimensional image[1]. In CT the x-ray source and the x-ray detector rotate 360 degrees about the object to get the complete set of projection data for the reconstruction of cross-sectional images, whereas in digital tomosynthesis projection data are taken over only a small span of rotation angle (for example 40-50 degree) with a limited number of x-ray exposures (for example 10-20). A reconstruction algorithm is then applied to obtain tomographic images from this limited projection data. As a result, tomosynthesis yields a significant reduction in imaging time, cost, and radiation dose to the patient.

In conventional motion tomography using x-ray films, the plane of focus depends on the fulcrum plane about which the x-ray detector and the x-ray source move on a given trajectory such as linear, circular or spiral trajectory. The reconstructed image on the fulcrum plane is well focused, whereas the images outside the fulcrum plane are linearly blurred according to the distance from the fulcrum plane. To obtain three dimensional images, multiple scans with the fulcrum points positioned on the plane of interest are necessary in conventional motion tomography. Multiple scans may result in excessive x-ray exposure and long scan time, which makes the motion tomography impractical for clinical application.

Digital tomosynthesis overcomes this problem by reconstructing arbitrary number of slices from the projection data acquired in a single scan. The key idea of digital tomosynthesis is to perform shift and add of the constituent projection images in a way that the structure on the given plane comes into focus while those on other planes are distributed over the image and appear blurred[1]. Tomosynthesis has been developed from the beginning of the twentieth century. Dobbins *et al.* described the history, various techniques, deblurring algorithms and clinical applications of tomosynthesis in details[1]. In 1970s, Grant implemented the technology and firstly coined the term tomosynthesis[2]. In late 1970s, the coded-aperture imaging was introduced to reduce the film-based tomosynthesis scan time[3,4]. The coded aperture imaging was named differently by various groups like, '*short-time tomosynthesis*'[5], '*flashing tomosynthesis*'[6-11] and '*tomoscopy*'[12]. Tomosynthesis was also tried using image intensifiers[13,14] which made the image acquisition and reconstruction more flexible. But tomosysnthesis using image intensifiers has not been widely used due to the limitations like geometric image distortion. In the late 1990s, the advent of the flat panel x-ray detector,

Corresponding Author : Soo Yeol Lee, Professor
Dept. of Biomedical Engineering Kyung Hee University, Korea
Tel : +82-31-201-2980 / Fax : +82-31-201-3666
E-mail : sylee01@khu.ac.kr
This study was supported by a grant of the Korea Health 21 R&D Project, Ministry of Health and Welfare (02-PJ3-PG6-EV07-0002) and a grant from the Korea Science and Engineering Foundation (R11-2002-103).

capable of providing high quality image at a rapid readout rate, expedited development of digital tomosynthesis. Moreover, effective deblurring algorithms[15-17] and fast computation speed make now digital tomosynthesis acceptable for the clinical purpose.

Recently, cone-beam CTs having flat-panel detectors have been introduced for the clinical use. Despite of excessive Compton scattering effects, cone beam CTs are now finding combinational applications of fluoroscopy, angiography and 3D tomographic scanning. In this study, we have obtained tomosynthesis images using a flat-panel detector based micro-CT which can be considered as a scale down version of a clinical cone-beam CT. The micro-CT has micron-resolution imaging capability and it has been greatly utilized in high resolution imaging of complex structural tissues such as trabecular bones[18] and micro vessels[19]. We show tomosynthesis images of multiple slices of a phantom reconstructed from the limited-angle projection data.

II. METHODS

A. Logarithm Transformation

The arriving x-ray intensity on the detector is proportional to the path integral of the attenuation coefficient along the path of the ray. Neglecting beam hardening and scattered radiation, the pixel intensity, I_{out}, on a detector element after attenuation along the line L will be,

$$I_{out} = I_{in} \cdot e^{-\sum_L \mu_i \Delta x_i} \tag{1}$$

In eq. (1) I_{in} is the incident x-ray intensity from the x-ray tube, and μ_i is the attenuation coefficient of the small element i of thickness Δx_i. After applying the logarithm transformation on eq. (1) and considering thickness Δx_i approaches zero, we can make a linear relation between the pixel intensity values and the integral of the attenuation coefficient values traversed,

$$-\ln\left(\frac{I_{out}}{I_{in}}\right) = \int_L \mu_i \Delta x_i \tag{2}$$

This linear transform is very essential because it ensures that the tomosynthesis image, generated by the linear combination of projection images, has a linear relationship to the object in the plane of interest and other off-focus planes.

B. Shift-and-add

The shift-and-add algorithm relies on the parallax effect. Depending on the different amounts of parallax experienced by tissue structures at different height above the detector, this algorithm shifts and adds in such a way that the structure in a given plane of interest all line up and thus be in focus. Typically three types of imaging geometry are considered, parallel, complete isocentric and partial isocentric as shown in Fig. 1.

In parallel geometry, assuming that the tube and detector move in synchrony in some pattern in parallel planes, the magnification of the objects depends only on their relative height z above the detector and not on the locations of the tube or detector within these two planes. In other words, the magnification of tissue structures within a given plane parallel to the detector plate remains constant in each of the projection images.

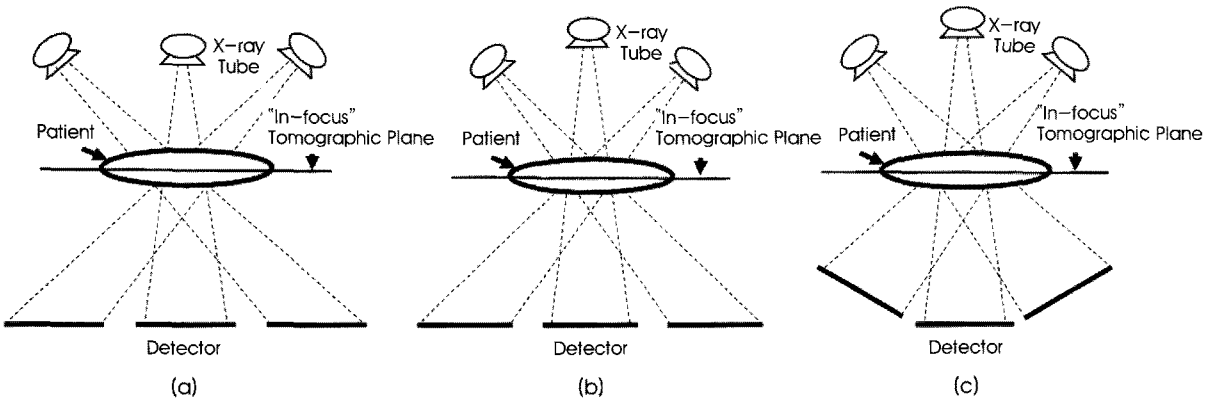

Fig. 1. Tomosynthesis geometries. (a) Parallel motion in which the source and the detector move in parallel to each other in opposite direction. (b) Partial isocentric motion in which the detector is stationary and the x-ray tube rotates about some rotation point. (c) Complete isocentric motion in which both the x-ray tube and the detector rotate about a fixed central point.

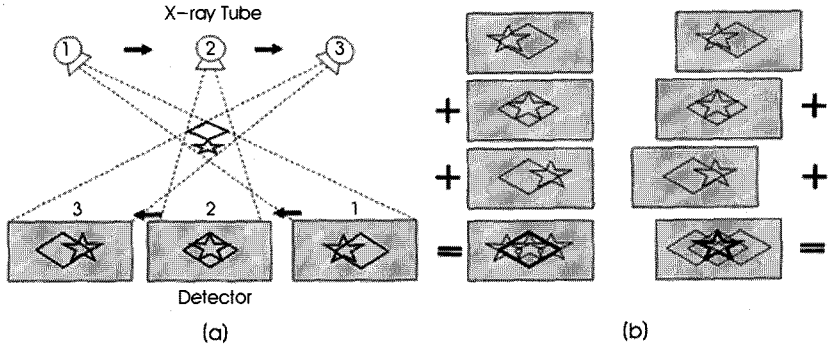

Fig. 2. The principle of shift-and-add tomosynthesis. (a) Projected locations of diamond and star at different height due to the different positions of the detector and the x-ray tube. (b) The acquired projection images are appropriately shifted and added to bring either diamond or star in focus, while structure outside the plane of focus blurred across the image.

The principle of shift-and-add algorithm can be understandable from Fig. 2. In Fig. 2(a), three different positions of the x-ray tube and the detector are shown. The diamond and the star overlay each other when x-ray tube is at location 2; while x-ray tube is at location 1 and 3 the projection of the objects are shifted relative to each other in the image plane. In Fig. 2, it is assumed that the diamond is located at the fulcrum plane. Hence, the diamond is always projected at the same location of the detector and the star is projected different positions of the detector. So, if all the projection images are simply added, then the diamond will be focused and the star will spread in the image. In case of focusing on the plane outside the fulcrum plane, appropriate shifting is required. In Fig. 2(b), the projection images are shifted to bring the star in focus. This simple shifting and adding illustrates the basic idea of tomosynthesis.

When the x-ray source and the detector do not move in parallel planes, as in the case of fully or partially isocentric geometry, the magnification of structures depends not only on their heights along the z-axis, but also on their tomographic angle. Before applying the shift-and-add procedure, it should be ensured that the magnification of any plane of interest remains constant in each of the projection images.

C. Isocentric Motion

Kolitsi *et al.* have shown mathematically that it is possible to render sharp focus of any arbitrary plane of the patient in the isocentric geometry [20]. Figure 3 represents the geometry for the isocentric motion. In the isocentric motion, the source and the detector rotate circularly in opposite direction maintaining a constant distance from the isocentre. In Fig. 3, a and b represent the distance between source-to-object and source-to-detector respectively, θ is the gantry angle and C is the isocentre. S_0 and S_θ are the source position at gantry angle 0° and θ°, respectively.

1) Plane of interest containing the isocentre

In Fig. 3, CD represents the horizontal plane which contains the isocentre and C_iD_i is the projected image on the detector plane for a specific gantry angle. The projected data C_iD_i must be converted to a plane $C_{hz}D_{hz}$ which is parallel to the plane of interest. Kolitsi *et al.* showed this transformation as below[20],

$$d_{hz} = \frac{d_i b}{b\cos\theta - d_i \sin\theta} \tag{3}$$

where d_{hz} represents, for any pixel, the distance from the origin of the detector to the projection position of that pixel on the horizontal plane, and d_i represents the distance from the origin to that pixel in the image receptor plane. In both cases, the origin is considered to be the projected location of the isocentre. It can be proved that the projection image length along the x-axis is constant for any gantry angle and there is no

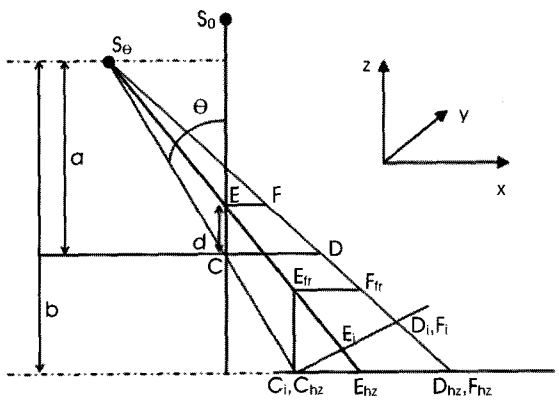

Fig. 3. Geometric representation of the shift-and-add tomosynthesis reconstruction.

longer any mismatch of the projection image length as a function of the gantry angle. So, if the projection images over all sampling angles add together, only structures in the plane of interest stay perfectly align, while structures outside the plane-of-interest are blurred.

2) Plane of interest outside the isocentre plane

Consider a plane of interest outside the isocentre plane, for example EF in Fig. 3, at a distance d above the isocentre. In order to get the focused image on EF plane, Kolitsi *et al.* showed some procedures[20]. Initially, transform the image receptor data to the horizontal plane parallel to the plane of interest *i.e.* $E_i F_i$ to $E_{hz} F_{hz}$; then perform the shifting (in Fig. 3, shift $E_{hz} F_{hz}$ so that E_{hz} is set to the origin of the image receptor); and finally, normalize the projected and shifted image to the magnification ratio of the isocentre plane. The first step is similar to the Eq. (3). Kolitsi *et al.* defined the last two steps as follows,

$$d_f = \left(d_{hz} - \frac{db\sin\theta}{a\cos\theta - d}\right)\left(1 - \frac{d}{a\cos\theta}\right) \qquad (4)$$

where d_f is the position in a fictitious plane ($E_f F_f$ is the fictitious plane in Fig. 3) for the pixel located at d_{hz} from the origin of the detector. In this fictitious plane, the structure of the plane of interest does not change as a function of gantry angle θ. So, addition of the transformed images, over all the gantry angles, will render the focused image of the plane EF. Kolitsi *et al.* also demonstrated that focal planes could be rendered at any orientation to the detector plane[20].

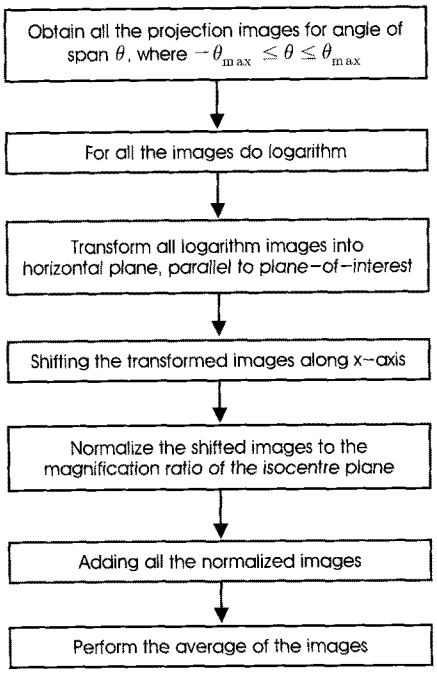

Fig. 4. Flow chart of the shift-and-add tomosynthesis reconstruction.

3) Flow-chart of shift-and-add tomosynthesis reconstruction

In Fig. 4 first three steps represent the acquisition of the projection images, performing logarithmic transformation, and then projection of the log data on the horizontal plane parallel to the plane of interest. The next two steps indicate shifting the projected horizontal data along x-axis depending on the distance of the plane of interest from the isocentre and adjusting the magnification. Finally, after performing these previous steps to all the projection images, the reconstructed tomosynthesis image on the desired plane is obtained.

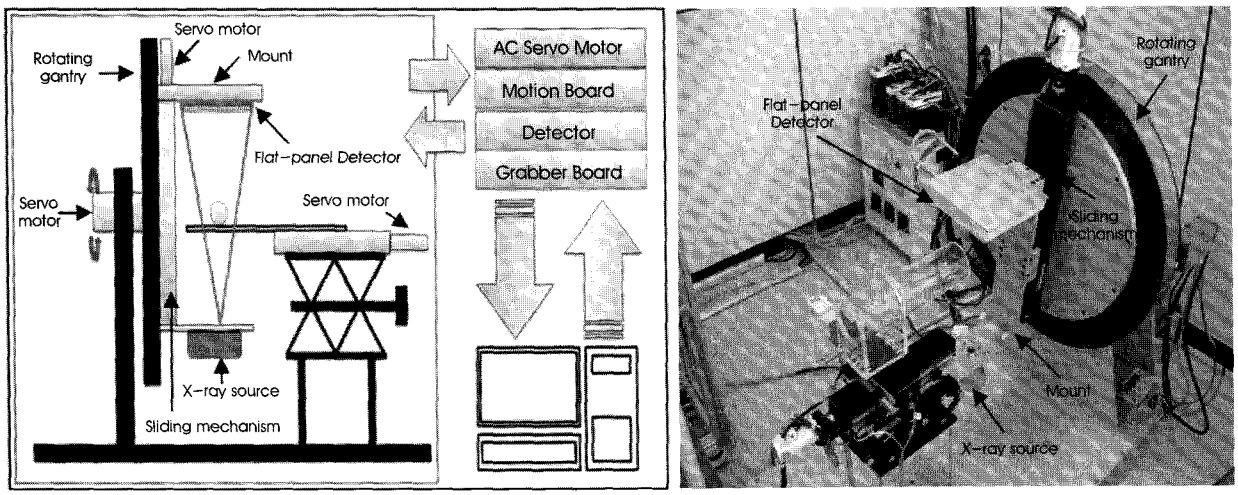

Fig. 5. (a) System configuration of the rotating gantry micro-CT system. (b) A photograph of the micro-CT system.

D. Micro-CT System

The micro-CT system has the rotating gantry structure on which the x-ray source and the detector are mounted. The rotating gantry has the diameter of 540 mm and thickness of 20 mm and it is composed of a circular aluminum plate. A servo motors, having the same 0.036 deg angular resolution, is used to rotate the gantry. The servo motor controls the rotating gantry with the angular resolution of 0.36×10^{-3} deg through 100:1 speed reduction gear. The distance from the x-ray source to the detector is 450mm and the distance from x-ray source to the object ranges from 91 mm to 380 mm. The magnification ratio can be varied from 1.2 to 5. Detailed configuration of the rotating gantry micro-CT system has been described in one of our previous studies[21].

A micro-focus x-ray source (5000 Apogee, Oxford Instrument, USA), with the nominal focal spot size of 35 mm, is on the mount facing the flat panel detector. The maximum tube voltage is 50 kVp, and the maximum tube current is 1 mA. When the x-ray is emitted, the micro-focus x-ray source operates in a continuous mode. We used a commercially available flat-panel detector (C7943CP-02, Hamamatus, Japan) which can obtain high resolution projection images of small objects such as rat. The flat-panel detector has a 1248 × 1248 active matrix of transistors and photodiodes with a pixel pitch of 100 μm. It has a CsI:TI scintillator and sensitive area of 12 cm × 12 cm. The host computer has Intel Core2 Quard Q6600 2.4 GHz processor, 3.5 GB physical memory and Windows XP operating system. The servo motor controller is connected through a motion control board (PCI-7354) made by National Instruments, TX, USA, and the detector is connected through image acquisition board (NI-1428) made by National Instruments, TX, USA.

III. SIMULATION RESULTS

We have developed a computer simulated program in MATLAB maintaining the same geometry of our rotating-gantry micro-CT system. Two small identical spheres, radius

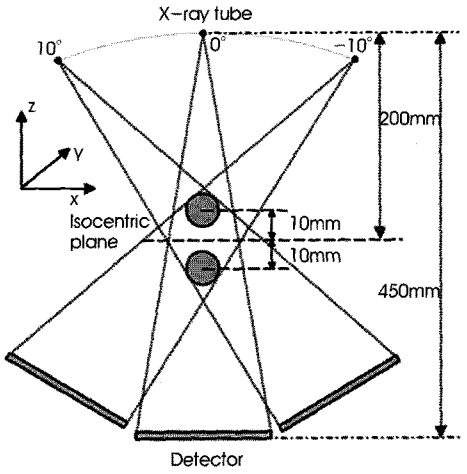

Fig. 6. Schematic representation of the geometry of the simulated micro-CT system

of 1 mm, located at opposite side of the isocentre along the z-axis, are considered as the object shown in Fig. 6. The center of each sphere is 10 mm far from the isocentre. Total of 20 projection images, over a tube angle of 20 degrees, starting from -10° to 10° for each degree, have been taken. The distance from x-ray source to isocentre and the x-ray source to the detector plate is 200 mm and 450 mm, respectively. Figure7(a) represents the projection images for various projection angles. The projection images of the spheres overlay each other when the gantry angle is 0° while for other gantry angles, the projected position is shifted relative to each other in the image plane. Figure7(b), in turn, shows three reconstruction at three different planes, at the center plane of the one sphere $(z = -10mm)$, at the center plane of another sphere $(z = 10mm)$ and at the isocentre plane $(z = 0mm)$, respectively, considering $z = 0$ as isocentre. When the plane-of-interest is $z = \pm 10mm$ as in Fig. 7(b), one of the spheres is in-focus whereas another sphere is out-of-focus. On the other hand, in the reconstructed image at $z = 10mm$ neither of the sphere is in-focus, consequently the shape is distorted.

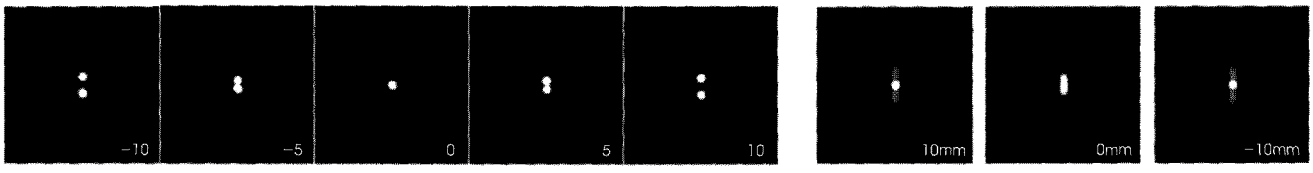

Fig. 7. (a) Simulated projection images. The spheres are projected differently on the image plane with different gantry angles (-10°, -5°, 0°, 5°, 10°). (b) Tomosynthesis images at the center plane of the upper sphere (z = 10mm), at the isocentre plane (z = 0mm) and at the center plane of lower sphere (z = -10mm), respectively.

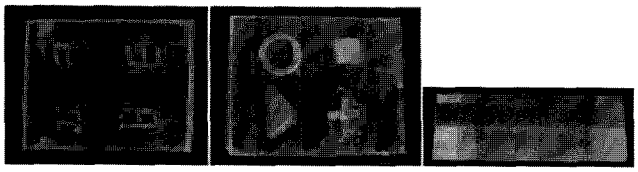

(a) (b) (c)

Fig. 8. Phantom made of acrylic, foam and copper sheet. (a) The plane containing Korean characters, facing towards the x-ray source during the experiment. (b) The plane containing basic geometric shapes, facing toward the detector. (c) thickness of 20mm.

Ⅳ. EXPERIMENTAL RESULTS

We have used a phantom, thickness of 20 mm, made of acrylic, foam and copper sheet as shown in Fig. 8. The phantom has two planes, one plane containing four basic geometric shapes and another one containing four Korean characters.The plane containing Korean characters has been facing towards the x-ray source. During the experiment comparing to the computer simulation, we used the same span of gantry angle and equal number of projection images as in Fig. 6.

The experimental image data taken at various projection angles from our micro-CT system are shown in Fig. 9. It is clearly visible that both the Korean character and the geometric structures are shifted and overlaid one another as the x-ray tube and the detector rotate. The reconstructed tomosynthesis images at various z-planes are shown in Fig. 10. We found that the best focused image at 5 mm above from the isocentre for the geometric symbol plane and at 15 mm below from the isocentre for the Korean character plane.

We compared the reconstructed images of the same plane with different projection angle spans. Fig. 11shows the synthesized image of the two planes of the phantom for two span angles, -10 to 10 degrees and -20 to 20 degrees. It can be noticed that wider span angle makes the out-of-focus plane more blurred out.

Ⅴ. DISCUSSION AND CONCLUSION

Cone beam CT provides high spatial resolution images using the projection data taken over 3600rotation of the x-ray

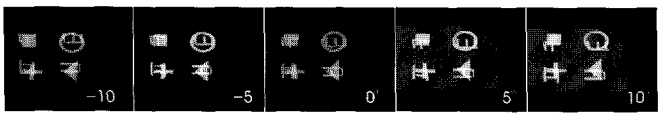

Fig. 9. The projection images of the phantom for various projection angles obtaining from the micro-CT system.

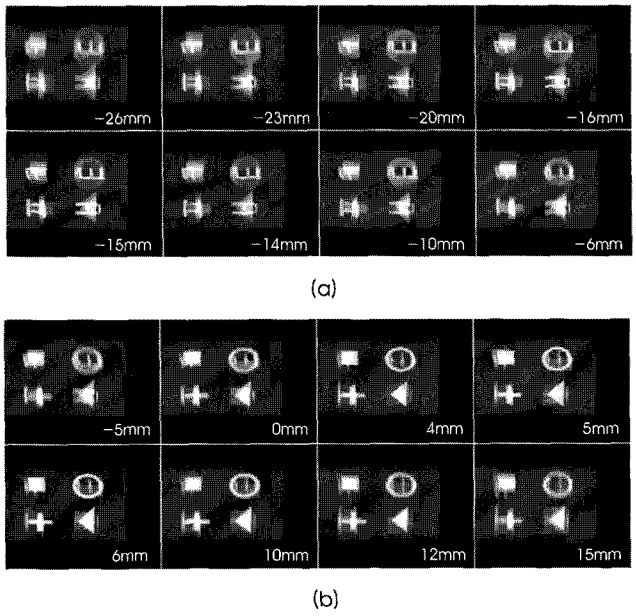

Fig. 10. (a) Reconstructed images at various planes from the isocentre along the z-axis. We found the best focused image (a) at 15mm below and (b) 5mm above the isocentre for the Korean character and the geometric symbol plane, respectively.

tube and the detector in complete isocentric geometry. On the contrary, digital tomosynthesis can provide appropriate image quality by using the projection data acquired over a limited projection angle in cone beam geometry. So, it would be clinically useful to exploit both the cone beam CT and the digital tomosynthesis in one imaging system so that we can choose any of the techniques depending on the image resolution, computational time and radiation dose. In this study, we applied the shift-and-add algorithm on our computer simulated phantom, as well as on the acquired experimental data of a simple phantom taken from our rotating-gantry-based micro CT system. In both cases, the structures on the plane of interest are well focused implying that a cone-beam CT can be used for digital tomosynthesis. However, as can be noticed from both simulation and experimental results, the shift-and-add

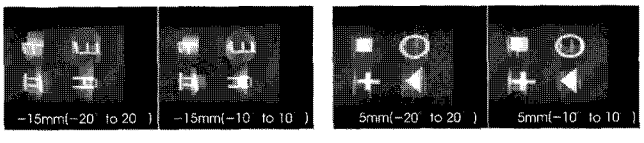

Fig. 11. Comparison between synthesize images using different number of projection images. (a) the in-focus Korean characters structure is clear; the structure of the geometric shape is more blurred for 20 images (-20° to 20°) than 10 images (-10° to 10°). (b) similar effect is shown when the plane-of-focus is geometric planes.

algorithm cannot remove completely the out-of-focus planes it merely blurs them onto the background. The other planes outside the plane-of-interest are only smeared out across the summed images, and superimposed on the plane of interest as noisy patterns. Various deblurring methods like Matrix Inversion Tomosynthesis (MITS), Filtered Back Projection (FBP), Ruttiman, Groenhuis and Webber (RGW) iterative method have been introduced[1]. It is known that MITS is faster and better for the high and mid frequency response, whereas it cannot remove completely the low-frequency noise. FBP works well for low-frequency noise. RGW iterative reconstruction method works fine when the number of iteration is large, but in that case computation time is long. So our future plan is to apply some deblurring algorithms to remove the noise completely from the reconstructed image.

REFERENCES

[1] J.T. Dobbins III and D.J. Godfrey, "Digital x-ray tomosynthesis: current state of the art and clinical potential", *Phys. Med. Biol.*, vol. 48, pp.R65-R106, 2003.

[2] D.G. Grant, "Tomosynthesis: a three-dimensional radiographic imaging technique", *IEEE Trans. Biomed. Eng.*, vol. 19, pp.20-28, 1972.

[3] E. Klotz and H. Weiss, "Three-dimensional coded aperture imaging using nonredundant point distributions", *Opt. Commun.*, vol. 11, pp.368-372, 1974.

[4] G. Groh, "Tomosynthesis and coded aperture imaging: new approaches to three-dimensional imaging in diagnostic radiography", *Proc. R. Soc. B*, vol. 195, pp.299-306, 1977.

[5] E. Klotz and H. Weiss, "Short-time tomosynthesis The New Image in Tomography", *in Proc. Symp. ActualitatisTomographiae, Genoa, Italy, Sept.* 1975, pp.11-13.

[6] M. Nadjmi, H. Weiss, E. Klotz and R. Linde, "Flashing tomosynthesisa new tomographic method", *Neuroradiology*, vol. 19, pp. 113-117, 1980.

[7] H. Becher, P. Hanrath, M. Schluter, W. Bleifeld, E. Klotz, P. Haaker, R. Linde and H. Weiss "Selective coronary angiography with flashing tomosynthesis in patients with coronary artery disease (abstract)", *Circulation* vol. 68 (Suppl III) pp.III-178, 1983.

[8] H. Becher, M. Schluter, D. G. Mathey, W. Bleifeld, E. Klotz, P. Haaker, R. Linde and H. Weiss "Coronary angiography with flashing tomosynthesis", *J. Eur. Heart*, vol. 6, pp.399-408, 1985.

[9] P. Haaker, E. Klotz, R. Koppe, R. Linde and D. G. Mathey, "First clinical results with digital flashing tomosynthesis in coronary angiography", *J. Eur. Heart*, vol. 6, pp.913-920, 1985.

[10] P. Haaker, E. Klotz, R. Koppe, R. Linde and H. Moller, "A new digital tomosynthesis method with less artifacts for angiography", *Med. Phys.*, vol. 12, pp.431-436, 1985.

[11] G.M. Stiel, L.S.G. Stiel, E. Klotz and C.A. Nienaber, "Digital flashing tomosynthesis: a promising technique for angiocardiographic screening", *IEEE Trans. Med. Imaging.*, vol. 12, pp. 314-321, 1993.

[12] H. Sklebitz and J. Haendle, "Tomoscopy: dynamic layer imagingwithout mechanical- movements", *J. Am. Roentgenol.*, vol. 140, pp.1247-1252, 1983.

[13] N.A. Baily, R.A. Keller, C.V. Jakowatz and A.C. Kak, "The capability of fluoroscopic systems for the production of computerized axial tomograms", *Invest. Radiol.*, vol. 11, pp.434 -439, 1976.

[14] N.A. Baily and T.D. Kampp, "Digitized longitudinal tomography", *Invest. Radiol.*, vol. 16, pp.126-32, 1981.

[15] D.J. Godfrey, H.P. McAdams and J.T. Dobbins III., "Optimization of the matrix inversion tomosynthesis (MITS) impulse response and modulation transfer function characteristics for chest imaging", *Med. Phys.*, vol. 33, pp.655-667, 2006.

[16] U.E. Ruttimann, R.A.J. Groenhuis and R.L. Webber, "Restoration of digital multiplane tomosynthesis by a constrained iteration method", *IEEE Trans. Med. Imaging.*, vol. 3, pp.141-148, 1984.

[17] G. Lauritsch and W.H. Harer, "A theoretical framework for filtered backprojection in tomosynthesis", *SPIE*, vol. 3338, pp.1127-1137, 1998.

[18] I.K. Chun, M.H. Cho, J.H. Park and S.Y. Lee, "In vivo trabecular thickness measurement in cancellous bones: longitudinal rat imaging studies", *Physiol. Meas.*, vol. 27, pp.695-702, 2006.

[19] S.M. Jorgensen, O. Demirkaya and E.L. Ritman, "Three-dimensional imaging of vasculature and parenchyma in intact rodent organs with X-ray micro-CT", *Am. J. Physiol.*, vol. 275, pp. H1103-H1114, 1998.

[20] Z. Kolitsi, V. Anastassopoulos, A. Scodras and N. Pallikarakis, "A multiple projection method for digital tomosynthesis", *Med. Phys.*, vol. 19, pp.1045-1050, 1992.

[21] S.Y. Lee, M.H. Cho, S.C. Lee, I.K. Chun and J.J. Park, "Small Animal X-ray Micro-CT with Zoom-in Imaging Capability", *in Proc. IEEE Nuclear Science Symposium Conference Record*, vol. 5, pp.M14-16, 2006.